Progress In Electromagnetics Research M, Vol. 55, 37–49, 2017

Mixed Signal-Based GLR Detector for FM Passive Bistatic Radar Target Detection

Mohammad Zamani and Abbas Sheikhi*

Abstract—This paper addresses the CFAR target detection in FM-based passive bistatic radars as a composite hypothesis testing problem, using the mixed signal model. The corresponding generalized likelihood ratio test (GLRT) is derived. It has less computational requirements with respect to the conventional GLRT-based detector, previously developed in the literature, due to the decrease in the row dimension of the interference matrix. The proposed detector is computationally efficient for tracking or short-range-radar applications in which a few range cells are surveyed. The theoretical and simulation-based analysis of detection performance and a thorough discussion on the computational complexity compared with that of the existing detectors are also provided.

1. INTRODUCTION

Passive bistatic radar (PBR) systems, using existing transmitters as transmitters of opportunity, have been vastly studied in recent years [1–6]. Since the transmitted signal is not known for the PBR systems, a dedicated channel referred to as the reference channel is used for the reception of the directly transmitted signal. At least one surveillance channel is also utilized to receive the target echoes which are contaminated by the noise and strong returns of direct signal and clutter/multipath [1, 2]. In general, a proper interference cancellation method should be applied to the surveillance channel signal prior to the computation of cross ambiguity function (CAF) in order to make target detection possible [1, 2]. The CAF, as a matched filter, provides the required integration gain and is followed by the application of an adaptive threshold such as the frequently used cell averaging constant false alarm rate (CA-CFAR) [1, 2].

Transversal adaptive filters such as the least mean squares (LMS) were the first interference cancellation methods presented in the literature [1]. Despite their computational efficiency, they are incapable of handling Doppler-spreading clutter scenarios appropriately. Later, the extensive cancellation algorithm (ECA) based on the projection of the surveillance channel signal onto the subspace orthogonal to the interference subspace was proposed [7] which significantly improves the performance of interference cancellation with respect to the transversal adaptive filters [8]. The sequential cancellation algorithm (SCA) as a sequential implementation of the ECA which progressively discovers the strongest delayed and Doppler-shifted versions of the reference channel signal in the surveillance channel signal to eliminate their effects was also developed in order to reduce the computational load of the ECA [7]. The ECA and SCA were extended so that after clutter and direct signal cancellation, the sequential detection of targets is performed, and hence the masking effects of the strongest target echoes on weaker targets due to the low peak-sidelobe level of the CAF are reduced [7]. In [2], a batched implementation of the SCA known as "the multistage processing algorithm", applied to low Doppler resolution scenarios, was discussed which leads to an improved and faster target detection and interference cancellation than the SCA [2]. While the previous mentioned works were intuitive

Received 25 December 2016, Accepted 8 February 2017, Scheduled 2 March 2017

* Corresponding author: Abbas Sheikhi (sheikhi.ab@gmail.com).

The authors are with the Department of Communications and Electronics, School of Electrical and Computer Engineering, Shiraz University, Shiraz, Iran.

in the case that no detection optimality or pseudo-optimality could be associated with them [9], a solution for the problem of simultaneous interference cancellation and CFAR detection for the general multi-target scenarios based on detection theory has been recently given in [9]. The work in [9] models the detection problem as a composite hypothesis test, derives the corresponding generalized likelihood ratio test (GLRT) and formulates the closed form expressions of detection and false alarm probabilities. It uses an iterative algorithm called imperative target positioning (ITP) to implement the detector in practice. It has also been shown that "the multistage processing algorithm" [2] due to the high CFAR loss of its local CA-CFAR thresholding has an inferior detection performance than the GLRT with embedded CFAR property, especially in close-targets scenarios [9]. It is mentioned that while the ECA [7] or the GLRT [9] can potentially be used regardless of the type of the signal of opportunity, for high-range-resolution PBRs based on high-bandwidth transmitted signals like the DVB-T (digital video broadcast-terrestrial) in which the clutter is distributed in several hundreds of range cells and the dimension of the interference subspace and the number of samples to be processed within the integration time are large they are not practically applicable. Hence, they were mainly applied to FM-based PBRs in the literature [9–11]. The GLRT, which is also proved to be the uniformly most powerful invariant (UMPI) detector [10], has been generalized for multiband FM-based PBRs [10] and is rewritten using the split received signal for the DVB-T-based PBR which is referred to as the GLRT-SS (GLRT with split signal) [11].

The detection performance of the GLRT has been compared with that of "the multistage processing algorithm" and the adaptive filter-based algorithms in [9–12] and [11, 12], respectively. According to the results of [9–12], the GLRT whose only limitation is its high computational complexity has much better detection performance than the existing methods. Hence, it is of a great interest to investigate detection tests which have detection performances close to that of the GLRT with less computational complexity. This is the main idea of this paper. In this regard, we investigate the problem of CFAR target detection in FM-based PBRs using the mixing product (mixed signal) model. The mixing product was previously used to implement the CAF to minimize the computational burden [13] and also to adopt space time adaptive processing (STAP) methods to airborne PBRs [14–16]. We use this signal model to derive a GLRT-based detector which is called M-GLRT throughout the manuscript to distinguish it from the existing GLRT [9, 10]. As will be demonstrated in the next sections, while the computational complexity of the GLRT does not depend on the length of surveillance range interval, the computational complexity of the M-GLRT is directly related to this length, and is substantially reduced for tracking or short-range-radar applications. In these cases, by a proper setting of the algorithm, the proposed M-GLRT needs less computational requirements than the GLRT but with a negligible detection loss, which is shown by the theoretical analysis and computer simulations.

The rest of the paper is organized as follows. Section 2 presents the signal model used to attain the hypothesis test. The detector design and its theoretical performance analysis as well as computational complexity are given in Section 3. Sections 4 and 5 are dedicated to the simulation results and conclusion, respectively.

Throughout this paper, $(.)^T$, $(.)^H$, $(.)^*$, $\odot$ and $\otimes$ represent the transpose, complex conjugate transpose, complex conjugate, Hadamard product and Kronecker product, respectively. For an arbitrary matrix $\mathbf{X}$, its kth vector column and its entry in row b and column c are denoted by $[\mathbf{X}]_k$ and $[\mathbf{X}]_{bc}$, respectively. $[\mathbf{x}]_k$ denotes the kth element of vector $\mathbf{x}$. S-dimensional unit and zero vectors are symbolized by $\mathbf{1}_S$ and $\mathbf{0}_S$, respectively. The N-dimensional identity matrix is written as $\mathbf{I}_N$. $||\mathbf{x}||$ denotes the Euclidean norm of vector $\mathbf{x}$.

2. SIGNAL MODEL

In this section, firstly the conventional signal model for PBRs according to [1–12] is introduced. Then, the mixed signal model which is the case in this paper is discussed.

In a PBR, the reference channel antenna is steered toward the transmitter to receive the direct signal. It is assumed that the multipath-free direct signal is available in the reference channel by some preprocessing such as channel equalization [17]. The nth sample of the direct signal after baseband demodulation is denoted by $d(n)$. The surveillance antenna receives the signal containing targets, clutter and the direct signal, received via its sidelobe or backlobe. It is assumed that the direct signal-

to-noise ratio (DNR) in the reference channel is much larger than the DNR in the surveillance channel, so that the thermal noise in the reference channel can be neglected [2, 9].

To formulate the surveillance channel signal, it is assumed that there are N_t targets with bistatic sample delays n_{t_k}, $k = 1, \ldots, N_t$ (with respect to the direct signal), complex amplitudes a_{t_k} and bistatic Doppler frequencies f_{t_k}. The clutter is modeled as a large number of scatterers distributed from bistatic sample delay (with respect to the direct signal) $r = 0$ to $N_r - 1$. N_c bistatic Doppler frequencies f_{c_i}, $i = 1, \ldots, N_c$ around the zero Doppler frequency are also considered for the clutter scatterers [9] in the general Doppler-spreading clutter case. The complex amplitude of the clutter scattrerer with bistaic sample delay r and Doppler frequency f_{c_i} is denoted by $\gamma_{c_{i,r}}$. The set of bistatic sample delays and Doppler frequencies assumed for the clutter scatterers is defined as "the clutter region" [9]. Thus, the surveillance channel signal, $x(n)$, can be written as [9]:

$$x(n) = \sum_{k=1}^{N_t} a_{t_k} d(n - n_{t_k}) e^{j2\pi f_{t_k}/f_s(n-1)} + \sum_{r=0}^{N_r-1} \sum_{i=1}^{N_c} \gamma_{c_{i,r}} d(n-r) e^{j2\pi f_{c_i}/f_s(n-1)} + w_s(n), \quad n = 1, \ldots, N \tag{1}$$

where $w_s(n)$ is the nth sample of the thermal noise in the surveillance channel, f_s denotes the sampling frequency and the number of samples to be processed within the integration time (T_i) is N. It is noted that the second term of Eq. (1) contains both the clutter and direct signal (corresponding to $r = 0, f_{c_i} = 0$). It is defined that

$$\begin{aligned} \mathbf{d} &= [\ d(1) \quad d(2) \quad \ldots \quad d(N)\ ]^T \\ \mathbf{w}_s &= [\ w_s(1) \quad w_s(2) \quad \ldots \quad w_s(N)\ ]^T \\ \mathbf{x} &= [\ x(1) \quad x(2) \quad \ldots \quad x(N)\ ]^T, \end{aligned} \tag{2}$$

as the vectors including the samples of $d(n)$, $w_s(n)$ and $x(n)$, respectively. The delayed version of $\mathbf{d}$ by r samples is denoted by $\mathbf{d}_r$. It can be computed by $\mathbf{D}^r\mathbf{d}$ where $\mathbf{D}$ is a 0/1 permutation matrix that applies one sample delay, and is defined by [9]:

$$\mathbf{D} = \{d_{ij}\}_{i,j=1,\ldots,N}, \quad d_{ij} = \begin{cases} 1 & i = j+1 \\ 0 & \text{otherwise} \end{cases} \tag{3}$$

$\mathbf{s}(f)$ as the temporal steering vector corresponding to Doppler frequency f is defined as:

$$\mathbf{s}(f) = \left[\ 1 \quad e^{j2\pi f/f_s} \quad \ldots \quad e^{j2\pi f/f_s(N-1)}\ \right]^T \tag{4}$$

So, the vector representation of Eq. (1) is given by:

$$\mathbf{x} = \mathbf{T}\mathbf{a}_t + \mathbf{C}\boldsymbol{\gamma} + \mathbf{w}_s \tag{5}$$

where

$$\begin{aligned} [\mathbf{T}]_k &= \mathbf{d}_{n_{t_k}} \odot \mathbf{s}(f_{t_k}), k = 1, \ldots, N_t \\ \mathbf{a}_t &= \left[\ a_{t_1} \quad a_{t_2} \quad \ldots \quad a_{t_{N_t}}\ \right]^T \\ [\mathbf{C}]_k &= \mathbf{d}_r \odot \mathbf{s}(f_{c_i}), k = rN_c + i \quad (r = 0, \ldots, N_r - 1, i = 1, \ldots, N_c) \\ \boldsymbol{\gamma} &= \left[\ \gamma_{c_{1,0}} \quad \gamma_{c_{2,0}} \quad \cdots \quad \gamma_{c_{N_c,0}} \quad \gamma_{c_{1,1}} \quad \cdots \quad \gamma_{c_{N_c,1}} \quad \cdots \quad \gamma_{c_{N_c,N_r-1}}\ \right]^T \end{aligned} \tag{6}$$

In other words, $\mathbf{a}_t$ contains the complex amplitudes of the targets, and $\boldsymbol{\gamma}$ is an N_rN_c-dimensional vector containing the complex amplitudes of the clutter scatterers (corresponding to all combinations of N_c Doppler frequencies and N_r sample delays) in such order that $[\boldsymbol{\gamma}]_{rN_c+i} = \gamma_{c_{i,r}}, r = 0, \ldots, N_r - 1, i = 1, \ldots, N_c$. The columns of $\mathbf{T}$ and $\mathbf{C}$ are the delayed and Doppler-shifted replicas of the direct signal which form a basis for N_t-dimensional targets and N_rN_c-dimensional clutter subspaces, respectively.

The mixing product (mixed signal) corresponding to sample delay (delay cell) m is defined as [13–16]:

$$\tilde{\mathbf{x}}(m) = \mathbf{x} \odot \mathbf{d}_m^* \tag{7}$$

It mixes the surveillance channel signal $\mathbf{x}$ with the complex conjugate of the mth sample-delayed version of the direct (reference) signal. Using Eq. (5) in Eq. (7) gives:

$$\tilde{\mathbf{x}}(m) = (\mathbf{T}\mathbf{a}_t + \mathbf{C}\boldsymbol{\gamma}) \odot \mathbf{d}_m^* + \mathbf{w}_{s_2}(m) \tag{8}$$

where

$$\mathbf{w}_{s_2}(m) \triangleq \mathbf{w}_s \odot \mathbf{d}_m^* \tag{9}$$

Let us define $\mathbf{T}_2(m)$ and $\mathbf{C}_2(m)$ such that $[\mathbf{T}_2(m)]_k = [\mathbf{T}]_k \odot \mathbf{d}_m^*, k = 1, \ldots, N_t$ and $[\mathbf{C}_2(m)]_k = [\mathbf{C}]_k \odot \mathbf{d}_m^*, k = 1, \ldots, N_r N_c$, then (8) is given by:

$$\tilde{\mathbf{x}}(m) = \mathbf{T}_2(m)\mathbf{a}_t + \mathbf{C}_2(m)\boldsymbol{\gamma} + \mathbf{w}_{s_2}(m) \tag{10}$$

Since the maximum Doppler frequency of targets, denoted by $f_{t_{\max}}$, is much smaller than the sampling frequency, the mixed signal is then applied to a low-pass filter (LPF) and subsampled by the subsampling factor S [13–16] to yield $\tilde{\mathbf{y}}(m)$ with $N_d = \lfloor N/S \rfloor$ samples. This process which does not affect the range resolution [14–16] can be implemented using the following low-pass filtering and subsampling (integrate-and-dump filtering) matrix:

$$\mathbf{S}_{N_d \times N} = \begin{pmatrix} \mathbf{1}_S & \mathbf{0}_S & \mathbf{0}_S & \ldots & \mathbf{0}_S \\ \mathbf{0}_S & \mathbf{1}_S & \mathbf{0}_S & \ldots & \mathbf{0}_S \\ \vdots & \ddots & \ddots & \ddots & \vdots \\ \mathbf{0}_S & \mathbf{0}_S & \ldots & \ldots & \mathbf{1}_S \end{pmatrix}^T = (\mathbf{I}_{N_d} \otimes \mathbf{1}_S)^T \tag{11}$$

where:

$$\begin{array}{l} \tilde{\mathbf{y}}(m) = \mathbf{S}\mathbf{D}^{-m}\tilde{\mathbf{x}}(m) = \mathbf{S}\mathbf{D}^{-m}(\mathbf{T}_2(m)\mathbf{a}_t + \mathbf{C}_2(m)\boldsymbol{\gamma} + \mathbf{w}_{s_2}(m)) = \mathbf{T}_3(m)\mathbf{a}_t + \mathbf{C}_3(m)\boldsymbol{\gamma} + \mathbf{w}_{s_3}(m), \\ \mathbf{S}\mathbf{D}^{-m}\mathbf{T}_2(m) \triangleq \mathbf{T}_3(m) \\ \mathbf{S}\mathbf{D}^{-m}\mathbf{C}_2(m) \triangleq \mathbf{C}_3(m) \\ \mathbf{S}\mathbf{D}^{-m}\mathbf{w}_{s_2}(m) \triangleq \mathbf{w}_{s_3}(m) \end{array} \tag{12}$$

i.e.,

$$[\tilde{\mathbf{y}}(m)]_b = \sum_{k=(b-1)S+1+m}^{bS+m} [\tilde{\mathbf{x}}(m)]_k, \quad b = 1, \ldots, N_d \tag{13}$$

N_d-dimensional vector $\tilde{\mathbf{y}}(m)$ is the subsampled mixed signal corresponding to sample delay m and it is to be analyzed. Since the bandwidth of the LPF is $\pm f_s/(2S)$ Hertz, S should be selected such that

$$f_{t_{\max}} \ll f_s/(2S) \tag{14}$$

to achieve negligible target signal-to-noise ratio (SNR) loss near cutoff frequency of the LPF. Since all target-related and clutter-related terms of $\tilde{\mathbf{y}}(m)$ share the same structure as a delayed and Doppler-shifted replica of the direct signal followed by mixing, filtering and subsampling, it is sufficient to investigate an arbitrary term such as the one related to the first target. This term which includes the signal contribution of the first target in $\tilde{\mathbf{y}}(m)$ is equal to $a_{t_1}[\mathbf{T}_3(m)]_1 = a_{t_1}[\mathbf{S}\mathbf{D}^{-m}\mathbf{T}_2(m)]_1$. Since

$$\begin{aligned} [\mathbf{S}\mathbf{D}^{-m}\mathbf{T}_2(m)]_{b1} &= \sum_{k=1}^{N} [\mathbf{S}]_{bk} [\mathbf{D}^{-m}\mathbf{T}_2(m)]_{k1} \\ &= \sum_{k=1}^{N} [\mathbf{S}]_{bk} d(k+m-n_{t_1}) d^*(k) e^{j2\pi f_{t_1}/f_s (k+m-1)} \\ &= e^{j2\pi f_{t_1}/f_s m} \sum_{k=(b-1)S+1}^{bS} d(k+m-n_{t_1}) d^*(k) e^{j2\pi f_{t_1}/f_s (k-1)} \\ &= e^{j2\pi f_{t_1}/f_s m} e^{j2\pi f_{t_1}/f_s S(b-1)} \sum_{k=1}^{S} d(k+(b-1)S+m-n_{t_1}) d^*(k+(b-1)S) e^{j2\pi f_{t_1}/f_s (k-1)}, \\ &\quad b = 1, \ldots, N_d \end{aligned} \tag{15}$$

it is concluded that:

$$\begin{aligned}
&a_{t_1}[\mathbf{T}_3(m)]_1 = a_{t_1}[\mathbf{S}\mathbf{D}^{-m}\mathbf{T}_2(m)]_1 = a'_{t_1}\mathbf{v}(f_{t_1}) \odot \mathbf{\Psi}(m-n_{t_1},-f_{t_1})\\
&[\mathbf{\Psi}(m-n_{t_1},-f_{t_1})]_b = \sum_{k=1}^{S} d(k+(b-1)S+m-n_{t_1})d^*(k+(b-1)S)e^{j2\pi f_{t_1}/f_s(k-1)}, \quad b=1,\ldots,N_d\\
&\mathbf{v}(f_{t_1}) = \left[\begin{array}{cccc} 1 & e^{j2\pi f_{t_1}S/f_s} & \ldots & e^{j2\pi f_{t_1}S(N_d-1)/f_s} \end{array}\right]^T\\
&a'_{t_1} \triangleq e^{j2\pi f_{t_1}/f_s m}a_{t_1}
\end{aligned} \tag{16}$$

$\mathbf{v}(f_{t_1})$ is in the form of the temporal steering vector of length N_d with Doppler frequency of f_{t_1} and the reduced sampling frequency of f_s/S. $\mathbf{\Psi}(m-n_{t_1},-f_{t_1})$ is an N_d-dimensional vector whose bth element, i.e., $[\mathbf{\Psi}(m-n_{t_1},-f_{t_1})]_b$ is the S-sample complex self-ambiguity function of the bth segment of $\mathbf{d}$ computed at sample delay of $m-n_{t_1}$ and Doppler frequency of $-f_{t_1}$. The magnitude of the S-sample complex self-ambiguity function corresponding to each of the segments has a correlation peak at sample delay-Doppler frequency pair of (0, 0) with the half-power Doppler correlation lobe width of $\pm f_s/(2S)$ Hertz and the half-power delay correlation lobe width of f_s/B samples, where B denotes the transmitting signal bandwidth [13].

If $m = n_{t_1}$, Eq. (16) simplifies to $a_{t_1}[\mathbf{T}_3(m)]_1 = a'_{t_1}\mathbf{v}(f_{t_1}) \odot \mathbf{\Psi}(0,-f_{t_1})$. The envelope of the direct signal whose kth sample is $|d(k)|^2$ is constant for FM signal: $|d(k)|^2 = A$. Using this representation, $\mathbf{\Psi}(0,-f_{t_1})$ is given by:

$$\begin{aligned}
[\mathbf{\Psi}(0,-f_{t_1})]_b &= \sum_{k=1}^{S}|d(k+(b-1)S)|^2 e^{j2\pi f_{t_1}/f_s(k-1)}, b=1,\ldots,N_d\\
&= A\sum_{k=1}^{S} e^{j2\pi f_{t_1}/f_s(k-1)} \triangleq l(f_{t_1}), b=1,\ldots,N_d \rightarrow\\
\mathbf{\Psi}(0,-f_{t_1}) &= l(f_{t_1})\mathbf{1}_{N_d}
\end{aligned} \tag{17}$$

According to Eq. (14), it can be shown that $|l(f_{t_1})| \cong AS$. Hence, if $m = n_{t_1}$, we have:

$$\begin{aligned}
a_{t_1}[\mathbf{T}_3(m)]_1 = a'_{t_1}\mathbf{v}(f_{t_1}) \odot \mathbf{\Psi}(0,-f_{t_1}) = a'_{t_1}l(f_{t_1})\mathbf{v}(f_{t_1}) = a''_{t_1}\mathbf{v}(f_{t_1}),\\
|a''_{t_1}| = |a'_{t_1}l(f_{t_1})| = |a_{t_1}|AS
\end{aligned} \tag{18}$$

which is a pure complex tone with the target Doppler frequency ($\mathbf{v}(f_{t_1})$) and proportional to the target complex amplitude. In the general case if $m \neq n_{t_1}$, according to Eq. (16) the contribution of the first target to $\tilde{\mathbf{y}}(m)$ is a modulated tone with an N_d-dimensional vector whose elements depend on the range profile of different segments' S-sample complex self-ambiguity functions.

The above discussion for the first target's signal contribution can be concluded as:

"$\tilde{\mathbf{y}}(m)$ is the summation of several pure tones corresponding to the targets and clutter scatterers at sample delay m, noise, and modulated tones due to the targets and clutter scatterers located at other sample delays."

$$\begin{aligned}
\tilde{\mathbf{y}}(m) \;=\; & a''_{t_j}\mathbf{v}(f_{t_j}) + \sum_{k=1,k\neq j}^{N_t} a'_{t_k}\mathbf{v}(f_{t_k}) \odot \mathbf{\Psi}(m-n_{t_k},-f_{t_k})\\
&+ \sum_{i=1}^{N_c}\gamma''_{c_{i,m}}\mathbf{v}(f_{c_i}) + \sum_{r=0,r\neq m}^{N_r-1}\sum_{i=1}^{N_c}\gamma'_{c_{i,r}}\mathbf{v}(f_{c_i}) \odot \mathbf{\Psi}(m-r,-f_{c_i}) + \mathbf{w}_{s_3}(m)
\end{aligned} \tag{19}$$

where it is defined that $\gamma'_{c_{i,r}} = \gamma_{c_{i,r}}e^{j2\pi f_{c_i}/f_s m}$ and $\gamma''_{c_{i,m}} = \gamma'_{c_{i,m}}l(f_{c_i})$, and it is assumed that the jth target is located at sample delay m in the clutter region. From Eq. (19), to compute $\mathbf{C}_3(m)$ for all m, $m = 1,\ldots,M$ the total number of distinct columns (tones or modulated tones) to be computed is $N_c(M+N_r)$. In this paper, the presence of a target at sample delay m in the presence of all these terms is to be investigated by processing $\tilde{\mathbf{y}}(m)$. To derive the detector, the statistical properties of the noise component of $\tilde{\mathbf{y}}(m)$, i.e., $\mathbf{w}_{s_3}(m)$ is required. As the thermal noise of the surveillance channel, i.e.,

$\mathbf{w}_s$ is a complex WGN [9] with level of σ^2 and according to Eqs. (7) and (12) all the transformations applied on the surveillance channel signal to derive $\tilde{\mathbf{y}}(m)$ are linear, $\mathbf{w}_{s_3}(m)$ will also have a zero-mean complex Gaussian distribution whose covariance matrix is given by:

$$\begin{aligned} E\{\mathbf{w}_{s_3}(m)\mathbf{w}_{s_3}(m)^H\} &= E\{(\mathbf{S}\mathbf{D}^{-m}\mathbf{w}_{s_2}(m))(\mathbf{S}\mathbf{D}^{-m}\mathbf{w}_{s_2}(m))^H\} \\ &= \mathbf{S}\mathbf{D}^{-m}E\{\mathbf{w}_{s_2}(m)\mathbf{w}_{s_2}(m)^H\}(\mathbf{D}^{-m})^H\mathbf{S}^H \\ &= \mathbf{S}\mathbf{D}^{-m}(E\{\mathbf{w}_s\mathbf{w}_s^H\} \odot (\mathbf{d}_m^*\mathbf{d}_m^T))(\mathbf{D}^{-m})^H\mathbf{S}^H \\ &= \sigma^2\mathbf{S}\mathbf{D}^{-m}diag(\mathbf{d}_m^*\mathbf{d}_m^T)(\mathbf{D}^{-m})^H\mathbf{S}^H = AS\sigma^2\mathbf{I}_{N_d} \triangleq \sigma'^2\mathbf{I}_{N_d} \end{aligned} \tag{20}$$

in which *diag* performs the matrix diagonalization, and $E\{.\}$ is the statistical expectation. Hence, $\mathbf{w}_{s_3}(m)$ is a complex WGN with variance of σ'^2, i.e., $N(\mathbf{0}_{N_d}, \sigma'^2\mathbf{I}_{N_d})$.

3. DETECTION ALGORITHM

Without loss of generality, the detection of a target with unknown complex amplitude a_t, known sample delay m and known Doppler frequency f_t in the presence of other targets, clutter and noise is modeled as a composite hypothesis test using Eq. (12) and the results of Eqs. (18) to (20), given by:

$$\begin{cases} \mathcal{H}_0 : a_t'' = 0 \\ \mathcal{H}_1 : a_t'' \neq 0 \end{cases} \tag{21}$$

or, equivalently

$$\begin{cases} \mathcal{H}_0 : \tilde{\mathbf{y}}(m) = \mathbf{U}(m)\boldsymbol{\theta} + \mathbf{w}_{s_3}(m) \\ \mathcal{H}_1 : \tilde{\mathbf{y}}(m) = a_t''\mathbf{v}(f_t) + \mathbf{U}(m)\boldsymbol{\theta} + \mathbf{w}_{s_3}(m) \end{cases} \tag{22}$$

where

$$\begin{aligned} &\boldsymbol{\theta} = [\boldsymbol{\gamma}^T \ [\mathbf{a}_t^T]_\alpha]^T \\ &\mathbf{U}(m) = [\mathbf{C}_3(m) \ [\mathbf{T}_3(m)]_\alpha] \\ &\mathbf{w}_{s_3}(m) \overset{d}{\sim} N(\mathbf{0}_{N_d}, \sigma'^2\mathbf{I}_{N_d}) \end{aligned} \tag{23}$$

$\boldsymbol{\theta}$ contains the complex amplitudes of the clutter scatterers and the interfering targets and is considered as a complex deterministic and unknown vector. a_t'' and σ'^2 are complex deterministic and unknown scalars. Since the clutter region is known a priori, $\mathbf{C}_3(m)$ is a known matrix whose columns span the clutter subspace in the mixed signal model. α denotes the indices of other (interfering) targets. So, the columns of $\mathbf{U}(m)$ span the interference (clutter and interfering targets) subspace and as mentioned before are in the form of a pure tone or modulated tone. For now, we assume that the number of the interfering targets and their sample delays and Doppler frequencies are known such that $\mathbf{U}(m)$ is a known $N_d \times (N_cN_r + N_t - 1)$ full column rank matrix which requires that $N_d > N_cN_r + N_t - 1 \triangleq P$. So, the number of samples for the subsampled mixed signal, i.e., N_d, is chosen larger than the dimension of the interference subspace, i.e., P. The method to sequentially determine the coordinates of the interfering targets is discussed later.

The hypothesis test given by Eq. (22) is the same as the conventional hypothesis test presented in [9, 10] except that the target signal and the interference matrix are modified based on the mixed signal model. We use the GLRT for this hypothesis test due to the unknown parameters a_t'' $\boldsymbol{\theta}$ and σ'^2 as derived in [9, 10]:

$$L_{M-GLRT}(\tilde{\mathbf{y}}(m)) = \frac{|\mathbf{v}(f_t)^H\mathbf{P}^\perp_{\mathbf{U}(m)}\tilde{\mathbf{y}}(m)|^2}{||\mathbf{P}^\perp_{\mathbf{U}(m)}\mathbf{v}(f_t)||^2||\mathbf{P}^\perp_{\mathbf{U}(m)}\tilde{\mathbf{y}}(m)||^2} \overset{\mathcal{H}_1}{>} \eta \tag{24}$$

where $\mathbf{P}^\perp_{\mathbf{U}(m)} = \mathbf{I}_{N_d} - \mathbf{U}(m)(\mathbf{U}(m)^H\mathbf{U}(m))^{-1}\mathbf{U}(m)^H$ is the orthogonal projection onto the subspace spanned by columns of $\mathbf{U}(m)$, and η is chosen according to the desired probability of false alarm, i.e., p_{fa}. This detector which is derived based on the mixed signal model by exploiting the GLRT is denoted

by M-GLRT. To derive the analytical detection performance of the M-GLRT, it can be shown that Eq. (24) is statistically equivalent to [9, 10]:

$$L'_{M-GLRT}(\tilde{\mathbf{y}}(m)) = \frac{N_d-(P+1)}{\frac{1}{L_{M-GLRT}(\tilde{\mathbf{y}}(m))}-1} \overset{\mathcal{H}_1}{>} \eta', \tag{25}$$

and in a similar way to [9, 10], it can be shown that:

$$L'_{M-GLRT}(\tilde{\mathbf{y}}(m)) \overset{d}{\sim} \begin{cases} F_{1,N_d-(P+1)} & \text{under} \quad \mathcal{H}_0 \\ F'_{1,N_d-(P+1)}(\delta) & \text{under} \quad \mathcal{H}_1 \end{cases} \tag{26}$$

where $F_{1,N_d-(P+1)}$ is a complex F distribution with 1 numerator complex degree of freedom and $N_d-(P+1)$ denominator complex degrees of freedom. $F'_{1,N_d-(P+1)}(\delta)$ denotes a non-central complex F distribution with 1 numerator complex degree of freedom, $N_d-(P+1)$ denominator degrees of freedom and non-centrality parameter $\delta = \frac{|a''_t|^2}{\sigma'^2}||\mathbf{P}^{\perp}_{\mathbf{U}(m)}\mathbf{v}(f_t)||^2$. Hence, the exact detection performance can be formulated by:

$$\begin{aligned} p_{fa} &= Q_{F_{1,N_d-(P+1)}}(\eta') \\ p_d &= Q_{F'_{1,N_d-(P+1)}(\delta)}(\eta') \end{aligned} \tag{27}$$

where

$$\eta = \eta'/(\eta' + N_d - (P+1)), \tag{28}$$

$Q_{F_{1,N_d-(P+1)}}(\eta')$ and $Q_{F'_{1,N_d-(P+1)}(\delta)}(\eta')$ are the right-tail probabilities of $F_{1,N_d-(P+1)}$ and $F'_{1,N_d-(P+1)}(\delta)$, respectively and p_d denotes the probability of detection. According to Eqs. (27) and (28), the threshold is independent of the unknown parameters and hence the CFAR property of the M-GLRT is satisfied. Using Eq. (27), it is seen that p_d is an increasing function of δ which can be interpreted as the output SNR in this paper, i.e., SNR_o. Since the input SNR, i.e., SNR_i, is equal to $|a_t|^2A/\sigma^2$, the SNR gain of the detector will be $\delta/SNR_i = ||\mathbf{P}^{\perp}_{\mathbf{U}(m)}\mathbf{v}(f_t)||^2S$.

If there exists no clutter scatterer or interfering target, the SNR gain is equal to $||\mathbf{I}_{N_d}\mathbf{v}(f_t)||^2S = N_dS$. On the other hand, due to the idempotent property of the orthogonal projection matrix [9, 18] it has either 0 or 1 eigenvalues, and it can be shown that [9, 18]:

$$0 \leq ||\mathbf{P}^{\perp}_{\mathbf{U}(m)}\mathbf{v}(f_t)||^2S \leq ||\mathbf{v}(f_t)||^2S = N_dS \tag{29}$$

So, in the presence of the interference the SNR gain is lower than the interference-free case, and we define the interference loss (IL) as follows:

$$IL = \frac{N_dS}{||\mathbf{P}^{\perp}_{\mathbf{U}(m)}\mathbf{v}(f_t)||^2S} = \frac{N_d}{||\mathbf{P}^{\perp}_{\mathbf{U}(m)}\mathbf{v}(f_t)||^2} \tag{30}$$

If the testing target coexists in the clutter region and interfering targets locations, $\mathbf{P}^{\perp}_{\mathbf{U}(m)}\mathbf{v}(f_t) = \mathbf{0}$ and $IL = \infty$. The coordinates close to that of the interference are also suffered by high IL. In other locations far enough from them, $||\mathbf{P}^{\perp}_{\mathbf{U}(m)}\mathbf{v}(f_t)||^2 \cong N_d$ which leads to negligible IL. So, the detector has a proper interference cancellation and target detection capability.

The derivation of the M-GLRT in Eq. (24) requires that the clutter region, number of interfering targets and their coordinates and hence $\mathbf{U}(m)$ are known. For clutter, this assumption is reasonable; but, for interfering targets it is not a practical one. So, initially the interference matrix consists of only the clutter region signals. The M-GLRT is evaluated for each sample delay-Doppler frequency pair in the desired sample delay-Doppler frequency plane outside the region of interference, and its maximum is compared with the predetermined detection threshold to find the strongest target. The coordinate of this target, which is an interfering target for the next targets, is used to update the interference matrix in the M-GLRT to cancel its effect and estimate the coordinate of the next strongest target. This procedure is repeated so that the coordinates of all targets are estimated sequentially. This is referred to as the ITP algorithm as in [9–11].

3.1. Implementation Issues of the ITP Algorithm

Since the M-GLRT should be computed many times (for every sample delay-Doppler pair) as mentioned above, some techniques are used to reduce its computational complexity:

1) The term $||\mathbf{P}^{\perp}_{\mathbf{U}(m)}\mathbf{v}(f_t)||^2$ in the denominator of Eq. (24) can be approximated as a constant value for targets whose coordinates are far from the interference region. We use this approximation for the whole detection plane to reduce the computational complexity [9–11].

2) The numerator of Eq. (24) for each m and a set of testing Doppler frequencies can be computed using the fast Fourier transform (FFT). We consider the number of FFT points to be $N_f = 2N_d$ corresponding to a set of testing Doppler frequencies spaced with half of Doppler resolution, i.e., $1/(2T_i)$.

Hence, the approximated version of the M-GLRT used in the ITP algorithm is given by:

$$\mathbf{l}_{M-GLRT}(\tilde{\mathbf{y}}'(m)) = \frac{FFT(\tilde{\mathbf{y}}'(m), N_f) \odot [FFT(\tilde{\mathbf{y}}'(m), N_f)]^*}{||\tilde{\mathbf{y}}'(m)||^2}, \quad m = 1, \ldots, M \tag{31}$$

where

$$\tilde{\mathbf{y}}'(m) \triangleq \mathbf{P}^{\perp}_{\mathbf{U}(m)}\tilde{\mathbf{y}}(m), \tag{32}$$

and sample delay M is corresponding to the maximum bistatic range of interest.

3) According to the math analysis in [10], $\mathbf{P}^{\perp}_{\mathbf{U}(m)}\tilde{\mathbf{y}}(m)$ in each iteration of the ITP algorithm can be computed using the previous iterations' results to avoid multiplication and inversion of larger matrices.

Hence, the detailed ITP algorithm for the M-GLRT detector using the idea of [10, 11] is given by:

Step 1: Set $l = 0$ and for all m $\mathbf{U}_0(m) = \mathbf{C}_3(m)$, $\mathbf{R}_0(m) = (\mathbf{C}_3(m)^H\mathbf{C}_3(m))^{-1}$ and $\tilde{\mathbf{y}}'_{-1}(m) = \tilde{\mathbf{y}}(m)$.

Step 2: For all m cancel the interference by:

$$\tilde{\mathbf{y}}'_l(m) = \mathbf{P}^{\perp}_{\mathbf{U}_l(m)}\tilde{\mathbf{y}}'_{l-1}(m) = \tilde{\mathbf{y}}'_{l-1}(m) - \mathbf{U}_l(m)\mathbf{R}_l(m)\mathbf{U}_l(m)^H\tilde{\mathbf{y}}'_{l-1}(m) \tag{33}$$

Step 3: Compute $\mathbf{l}^l_{M-GLRT}(\tilde{\mathbf{y}}'_l(m)), m = 1, \ldots, M$ using Eq. (31).

Step 4: The coordinate corresponding to the maximum value of $\mathbf{l}^l_{M-GLRT}(\tilde{\mathbf{y}}'_l(m))$ over m and f_t is the estimation of the coordinate of an interfering target if the exact M-GLRT given by Eq. (24), i.e., L_{M-GLRT} evaluated at this coordinate exceeds the threshold η, given by (28). Otherwise, the algorithm stops. If we denote this maximum by $\hat{c}$ and the corresponding coordinate by $(\hat{m}, \hat{f}_t)$, the exact M-GLRT evaluated at this coordinate is equal to $\hat{c}/||\mathbf{P}^{\perp}_{\mathbf{U}(\hat{m})}\mathbf{v}(\hat{f}_t)||^2$ where $\mathbf{P}^{\perp}_{\mathbf{U}(\hat{m})}\mathbf{v}(\hat{f}_t)$ is computed by [10]:

$$\mathbf{P}^{\perp}_{\mathbf{U}(\hat{m})}\mathbf{v}(\hat{f}_t) = \left[\prod_{s=0}^{l}\mathbf{P}^{\perp}_{\mathbf{U}_s(\hat{m})}\right]\mathbf{v}(\hat{f}_t) = \mathbf{v}(\hat{f}_t) - \sum_{s=0}^{l}\mathbf{U}_s(\hat{m})\mathbf{R}_s(\hat{m})\mathbf{U}_s(\hat{m})^H\mathbf{v}(\hat{f}_t) \tag{34}$$

Since $N_d \gg P$, it can be shown that the probability of false alarm does not change considerably with respect to the number of interfering targets and hence the threshold can be set a priory based on the desired probability of false alarm with an assumed maximum number of targets [9–11].

Step 5: Set $l = l + 1$ and register the extracted coordinate at the previous step as the estimated coordinate of the lth interfering target, i.e., $(\hat{m}, \hat{f}_t)^l$. Produce the lth interfering target matrix, i.e., $\mathbf{T}_{3,l}(m)$ (for all m) using $(\hat{m}, \hat{f}_t)^l$ with a proper N_b-cell mask around it for compensating any inaccuracy in the estimation. It is noted that each column of $\mathbf{T}_{3,l}(m)_{N_d \times N_b}$ as in Eq. (12) is a delayed and Doppler-shifted version of $\mathbf{d}$ based on the estimated and mask coordinates, followed by mixing, filtering and subsampling.

Step 6: Compute and store the matrices $\mathbf{U}_l(m)$ and $\mathbf{R}_l(m)$ (for all m), defined as:

$$\mathbf{U}_l(m) = \mathbf{T}_{3,l}(m) - \sum_{s=0}^{l-1}\mathbf{U}_s(m)\mathbf{R}_s(m)\mathbf{U}_s(m)^H\mathbf{T}_{3,l}(m) \tag{35}$$

$$\mathbf{R}_l(m) = (\mathbf{U}_l(m)^H\mathbf{U}_l(m))^{-1} \tag{36}$$

Step 7: Iterate Steps 2–6 until the algorithm stops.

By the end of the ITP algorithm, the unknown targets' parameters are estimated, and the exact threshold to set the desired false alarm probability and $\mathbf{T}_3(m) = [\ \mathbf{T}_{3,1}(m)\ \ \mathbf{T}_{3,2}(m)\ \ \ldots\ \ \mathbf{T}_{3,N_t}(m)\ ]$ can be computed. As a confirmation stage and to reduce the false alarms, each of the targets is considered as a testing target, while other targets (and the masks around them) are considered as interfering targets. Then, we employ the exact M-GLRT given by Eq. (24) using $\mathbf{U}(m) = [\mathbf{C}_3(m)\ [\mathbf{T}_3(m)]_\alpha]$.

3.2. Computational Complexity Analysis

In this section, the M-GLRT is compared with the conventional GLRT and GLRT-SS in terms of computational complexity. The GLRT for the conventional signal model, given by Eq. (5), evaluated at sample delay-Doppler pair of (m, f_t) can be written as [9, 10]:

$$L_{GLRT}(\mathbf{x}) = \frac{|(\mathbf{s}(f_t) \odot \mathbf{d}_m)^H \mathbf{P}_{\mathbf{U}}^{\perp} \mathbf{x}|^2}{||\mathbf{P}_{\mathbf{U}}^{\perp}(\mathbf{s}(f_t) \odot \mathbf{d}_m)||^2 ||\mathbf{P}_{\mathbf{U}}^{\perp}\mathbf{x}||^2} \tag{37}$$

where $\mathbf{U} = [\mathbf{C}\ [\mathbf{T}]_\alpha]_{N\times P}$. The approximated version of Eq. (37) used in the ITP algorithm is given by [9, 10]:

$$\mathbf{l}_{GLRT}(\mathbf{x}, m) = \frac{FFT(\mathbf{d}_m^* \odot \mathbf{P}_{\mathbf{U}}^{\perp}\mathbf{x}, N_f) \odot [FFT(\mathbf{d}_m^* \odot \mathbf{P}_{\mathbf{U}}^{\perp}\mathbf{x}, N_f)]^*}{||\mathbf{P}_{\mathbf{U}}^{\perp}\mathbf{x}||^2}, \quad m = 1, \ldots, M \tag{38}$$

where a decimation filter can be applied before the FFT computation [9, 10].

The GLRT-SS is another representation of the GLRT where the direct and surveillance channel signals are divided into K batches. The clutter matrix $\mathbf{C}$ and the targets matrix $\mathbf{T}$ are also generated as $\mathbf{C} = [\ \mathbf{C}^{1^T}\ \ \mathbf{C}^{2^T}\ \ \ldots\ \ \mathbf{C}^{K^T}\ ]^T$ and $\mathbf{T} = [\ \mathbf{T}^{1^T}\ \ \mathbf{T}^{2^T}\ \ \ldots\ \ \mathbf{T}^{K^T}\ ]^T$ based on the sub-matrices corresponding to the different batches denoted by $\mathbf{C}^k$ and $\mathbf{T}^k, k = 1, \ldots, K$, respectively [11].

Table 1 lists the operations with the required complex additions and products for the lth iterations of the ITP algorithms of the GLRT, GLRT-SS and M-GLRT detectors. In this table, P_0 is defined as $P_0 \triangleq N_r N_c$. It is noted that for the M-GLRT, since the operations are performed for each sample delay m individually, M as the total number of surveillance sample delays appears in the computational complexity expressions. But, for the GLRT and the GLRT-SS the main complexity does not depend on M.

4. SIMULATION RESULTS

In this section, several simulations are performed to show the effectiveness of the proposed M-GLRT and investigate its detection performance and computational complexity. The M-GLRT can be applied to all PBR systems using any signal of opportunity. Here, we choose FM radio broadcast signal as the transmitting signal for the simulations. The sampling frequency and the integration time are $f_s = 192\,\text{kHz}$ and $T_i = 1\,\text{s}$, respectively. It is assumed that the input DNR in the reference and the surveillance channels are 65 dB and 45 dB, respectively. It can be assumed that the clutter scatterers for FM-based PBRs are distributed in the bistatic ranges between 0 km and 55 km, and their input clutter-to-noise ratios (CNR_i) vary in the range of 5 dB to 35 dB [2, 9]. Hence, in the simulations, we consider ten clutter scatterers according to Table 2. The clutter region for the cancellation is also considered to be the first 37 sample delays corresponding to 56 km and Doppler frequencies of $\{-0.5, -0.25, 0, 0.25, 0.5\}$ Hz. In the ITP algorithm and the confirmation stage, the mask coordinates around each interfering target coordinate $(\hat{m}, \hat{f}_t)$ is comprised of three sample delays $\{\hat{m}, \hat{m} \mp 1\}$ and seven Doppler frequencies $\{\hat{f}_t, \hat{f}_t \mp q(f_s/S)/(6N_f)\}$, $q = 0,\ 1,\ 2,\ 3$ equivalent to total $N_b = 21$ range-Doppler cells which is shown to be adequate for compensating the target parameter estimation error [9, 10]. The maximum bistatic Doppler frequency of interest is $f_{t_{\max}} = 100\,\text{Hz}$ and the detection threshold is set for $p_{fa} = 10^{-6}$.

4.1. Evaluation of Detection Performance

In the first simulation scenario, the interference loss defined in Eq. (30) is investigated for the proposed detector. An interfering target is placed at bistatic range of 25 km and Doppler frequency of 20 Hz with

Table 1. Complexity (in terms of complex additions and products) of operations for the lth iterations of the ITP algorithms of the GLRT, GLRT-SS and M-GLRT.

Operation of GLRT - - - - - - - - **GLRT-SS**	**Complexity of GLRT/GLRT-SS**	**Operation of M-GLRT**	**Eq.**	**Complexity of M-GLRT**
-	-	Produce $\tilde{\mathbf{x}}(m)$ (M times)	(7)	MN
-	-	$\tilde{\mathbf{y}}(m) = \mathbf{S}\mathbf{D}^{-m}\tilde{\mathbf{x}}(m)$ (M times)	(13)	$M(N - N_d)$
Clutter matrix generation, $\mathbf{U}_0 = \mathbf{C}_{N\times P_0}$ - - - - - - $\mathbf{U}_0^k = \mathbf{C}^k, k = 1, \ldots, K$	$P_0 N$	Clutter matrix generation for all m, $\mathbf{U}_0(m) = \mathbf{C}_3(m)$	(19)	$(P_0 + N_c M)(3N - N_d)$
$\mathbf{R}_0 = (\mathbf{C}^H\mathbf{C})^{-1}$	$P_0^2(2N-1) + 1.3P_0^3$	$\mathbf{R}_0(m) = (\mathbf{C}_3(m)^H\mathbf{C}_3(m))^{-1}$ (M times)		$MP_0^2(2N_d - 1) + 1.3MP_0^3$
$\mathbf{a} = \mathbf{U}_l^H\mathbf{y}_{l-1}$ ($\mathbf{y}_{-1} = \mathbf{x}$) - - - - - - - $\mathbf{a} = \sum_{k=1}^{K} \mathbf{U}_l^{kH}\mathbf{y}_{l-1}^k$	$l = 0, P_0(2N-1)$	$\mathbf{a} = \mathbf{U}_l(m)^H\tilde{\mathbf{y}}'_{l-1}(m)$ (M times) ($\tilde{\mathbf{y}}'_{-1}(m) = \tilde{\mathbf{y}}(m)$)	(33)	$l = 0, MP_0(2N_d - 1)$
	$l > 0, N_b(2N-1)$			$l > 0, MN_b(2N_d - 1)$
$\mathbf{b} = \mathbf{R}_l\mathbf{a}$	$l = 0, P_0(2P_0 - 1)$	$\mathbf{b} = \mathbf{R}_l(m)\mathbf{a}$ (M times)	(33)	$l = 0, MP_0(2P_0 - 1)$
	$l > 0, N_b(2N_b - 1)$			$l > 0, MN_b(2N_b - 1)$
$\mathbf{c} = \mathbf{U}_l\mathbf{b}$ - - - - - $\mathbf{c}^k = \mathbf{U}_l^k\mathbf{b}$	$l = 0, N(2P_0 - 1)$	$\mathbf{c} = \mathbf{U}_l(m)\mathbf{b}$ (M times)	(33)	$l = 0, MN_d(2P_0 - 1)$
	$l > 0, N(2N_b - 1)$			$l > 0, MN_d(2N_b - 1)$
$\mathbf{y}_l = \mathbf{y}_{l-1} - \mathbf{c}$	N	$\tilde{\mathbf{y}}'_l(m) = \tilde{\mathbf{y}}'_{l-1}(m) - \mathbf{c}$ (M times)	(33)	MN_d
$\mathbf{d} = \text{decimate}(\mathbf{d}_m^* \odot \mathbf{y}_l, S)$ $\mathbf{e} = \text{FFT}(\mathbf{d}, 2N_d)$ (M times)	$MN + M(N - N_d)$ $+3MN_d\log_2(2N_d)$	$\mathbf{d} = \text{FFT}(\tilde{\mathbf{y}}'_l(m), 2N_d)$ (M times)	(31)	$3MN_d\log_2(2N_d)$
$a = \|\|\mathbf{y}_l\|\|^2$	$2N - 1$	$a = \|\|\tilde{\mathbf{y}}'_l(m)\|\|^2$ (M times)	(31)	$M(2N_d - 1)$
$\mathbf{l}^l_{\text{GLRT}}(\mathbf{y}_l, m) = \mathbf{e} \odot \mathbf{e}^*/a$ (M times) - - - - - $\mathbf{l}^l_{\text{GLRT-SS}}(\mathbf{y}_l, m) = \mathbf{e} \odot \mathbf{e}^*/a$	$4MN_d$	$\mathbf{l}^l_{M-GLRT}(\tilde{\mathbf{y}}'_l(m)) = \mathbf{d} \odot \mathbf{d}^*/a$ (M times)	(31)	$4MN_d$
-	-	$\hat{c}/\|\|\mathbf{P}^{\perp}_{\mathbf{U}(\hat{m})}\mathbf{v}(\hat{f}_t)\|\|^2$	(34)	$P_0(2N_d - 1) + P_0(2P_0 - 1)$ $+N_d(2P_0 - 1) + l\times$ $[N_b(2N_d - 1) + N_b(2N_b - 1)$ $+N_d(2N_b - 1)] + (l + 1)N_d$
lth target matrix generation, $\mathbf{T}_{l_{N\times N_b}}$	$N_b N$	lth target matrix generation, $\mathbf{T}_{3,l}(m)_{N_d\times N_b}$($M$ times)	(12)	$N_b N + M(2N - N_d)N_b$
$\mathbf{U}_l = \mathbf{T}_l - \sum_{s=0}^{l-1}[\mathbf{U}_s\mathbf{R}_s$ $\times\mathbf{U}_s^H\mathbf{T}_l]$ - - - - - $\mathbf{U}_l^k = \mathbf{T}_l^k - \sum_{s=0}^{l-1}[\mathbf{U}_s^k\mathbf{R}_s$ $\times \sum_{i=1}^{K} \mathbf{U}_s^{iH}\mathbf{T}_l^i]$	$P_0(2N-1)N_b + P_0(2P_0-1)N_b$ $+N(2P_0 - 1)N_b + (l-1)\times$ $[(2N-1)N_b^2 + (2N_b - 1)N_b^2$ $+N(2N_b - 1)N_b] + lNN_b$	$\mathbf{U}_l(m) = \mathbf{T}_{3,l}(m) - \sum_{s=0}^{l-1}[\mathbf{U}_s(m)$ $\times\mathbf{R}_s(m)\mathbf{U}_s(m)^H\mathbf{T}_{3,l}(m)]$ (M times)	(35)	$\{P_0(2N_d-1)N_b + P_0(2P_0-1)N_b$ $+N_d(2P_0 - 1)N_b + (l-1)\times$ $[(2N_d-1)N_b^2 + (2N_b - 1)N_b^2$ $+N_d(2N_b - 1)N_b] + lN_dN_b\}M$
$\mathbf{R}_l = (\mathbf{U}_l^H\mathbf{U}_l)^{-1}$	$N_b^2(2N-1) + 1.3N_b^3$	$\mathbf{R}_l(m) = (\mathbf{U}_l(m)^H\mathbf{U}_l(m))^{-1}$ (M times)	(36)	$MN_b^2(2N_d - 1) + 1.3MN_b^3$

Table 2. Specifications of clutter.

Scatterer number	*1*	*2*	*3*	*4*	*5*	*6*	*7*	*8*	*9*	*10*
Sample delay	1	4	8	12	16	16	20	24	28	31
Doppler, Hz	0	0	0.25	0	0	−0.25	0	0	0.5	0
CNR_i, *dB*	35	33	25	25	20	15	15	10	10	5

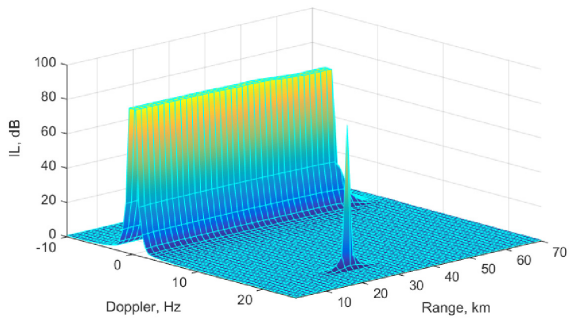

Figure 1. Two-dimensional plot of the interference loss.

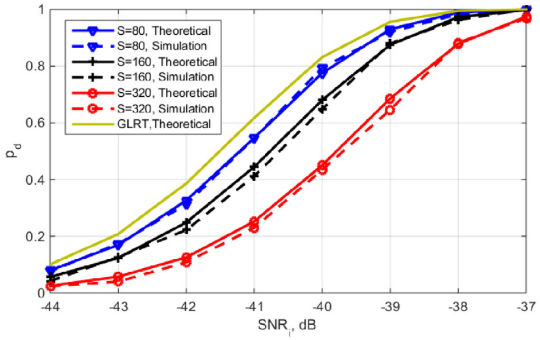

Figure 2. p_d versus SNR_i for the M-GLRT (with different values of S) compared with that of the GLRT for $p_{fa} = 10^{-6}$.

$SNR_i = -10$ dB. Fig. 1 shows the interference loss in the range-Doppler plane for subsampling factor $S = 160$. As can be seen, at coordinates corresponding to that of the clutter region and the interfering target IL is very high (about 84 dB) which is enough in practical situations. Also, in other coordinates far enough from them IL is negligible (about 0.7 dB).

For this scenario, a testing target is placed at bistatic range of 50 km and Doppler frequency of 35 Hz far from the interfering target. The Monte Carlo simulation-based and the theoretical detection performances of the confirmation stage for the M-GLRT are shown in Fig. 2 for $S = 80$, $S = 160$ and $S = 320$. As can be seen, the theoretical and simulation results match with each other. It is seen that the increase of S leads to a degraded performance. Since for an acceptable performance it is required that $N_d \gg P$, we recommend $S = 160$ for our FM-based PBR simulation. It is reminded that selecting lower values of S such as $S = 80$ may not be suitable since the computational complexity is increased as will be seen later. In this figure, the theoretical detection performance of the GLRT is also depicted. For $S = 160$, there is a negligible detection loss (about 0.7 dB) in the detection performance of the M-GLRT compared with that of the GLRT.

In the next simulation, a more difficult multi-target scenario is considered. In this scenario, targets 1 and 2 are close in range with the same Doppler frequency, and targets 2 and 3 are close in Doppler with the same range. The specifications of targets are listed in Table 3. The ITP algorithm and then the confirmation stage are employed and the detection probabilities of both the M-GLRT (with $S = 160$) and the GLRT versus the input SNR are plotted in Fig. 3 for all targets. To compute the testing target's probability of detection for a range of input SNRs, the input SNRs of other targets are chosen according to Table 3. As can be seen, the M-GLRT detects all targets well and compared with the GLRT it has at most 1.5 dB detection loss at $p_d = 0.8$ for targets 1 and 2.

4.2. Computational Complexity Comparison

The number of ITP iterations for the M-GLRT and GLRT is generally the same as that of the targets, i.e., N_t. Using Table 1, the computational complexity of the ITP algorithm for the GLRT, i.e., C_{GLRT}, divided by that of the M-GLRT, i.e., C_{M-GLRT} versus M, is shown in Fig. 4 for $S = 160$ and three different values of N_t. It can be seen that for any number of targets the M-GLRT is less computationally

Table 3. Specifications of targets in the second scenario.

Target number	T_1	T_2	T_3
Bistatic Range, km	7.03	17.97	17.97
Bistatic Doppler, Hz	22.00	22.00	14.50
SNR_i, dB	12	-14	-32

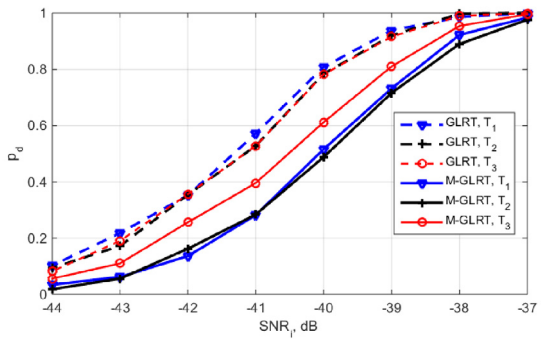

Figure 3. Detection performance comparison of the M-GLRT and the GLRT for $p_{fa} = 10^{-6}$ where T_k denotes the kth target in the second scenario ($S = 160$).

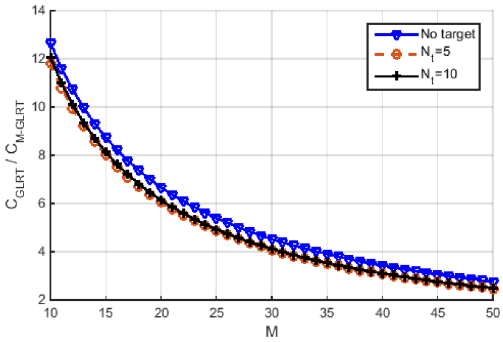

Figure 4. Ratio of C_{GLRT} to C_{M-GLRT} versus M(the maximum sample delay of interest) for $S = 160$.

intensive than the GLRT especially for short-range-radar applications (small values of M). For example, if $M = 30$ equivalent to bistatic range of 45 km, the ITP algorithm of the M-GLRT is approximately four times faster than that of the GLRT. Table 4 lists the approximated C_{GLRT}/C_{M-GLRT} for different values of S and $M = 30$. Using Fig. 2, the approximated detection loss of the M-GLRT with respect to the GLRT at $p_d = 0.8$ is also given in this table. As can be seen, there is a trade-off between detection performance and computational complexity depending on S.

Table 4. Trade-off between detection performance and computational complexity depending on S for $M = 30$.

Subsampling factor, i.e, S	Computational load saving factor of the M-GLRT, i.e., C_{GLRT}/C_{M-GLRT}	Detection loss of the M-GLRT, dB
80	2.3	0.3
160	4	0.7
320	6.6	1.6

5. CONCLUSION

In this paper, the GLR detector in the presence of direct signal, interfering targets, clutter and noise based on the mixed signal model is proposed. The detection probability of the proposed detector is derived theoretically and evaluated in the simulations. It is shown that its detection performance is slightly degraded compared with that of the conventional GLRT, but it can be several times faster depending on the maximum surveillance range of a PBR. Like the conventional GLRT, the proposed detector is shown to be capable of handling multi-target scenarios appropriately and hence is superior to the ad-hoc methods which are not designed based on detection theory and suffer from high detection losses in these scenarios.

REFERENCES

1. Cherniakov, M., *Bistatic Radar: Emerging Technology*, Wiley, 2008.
2. Colone, F., D. W. Ohagan, P. Lombardo, and C. J. Baker, "A multistage processing algorithm for disturbance removal and target detection in passive bistatic radar," *IEEE Transactions on Aerospace and Electronic Systems*, Vol. 45, No. 2, 698–722, 2009.
3. De Maio, A., G. Foglia, N. Pasquino, and M. Vadursi, "Measurement and comparative analysis of clutter for GSM and UMTS passive radars," *IET Radar, Sonar & Navigation*, Vol. 4, No. 3, 412–423, 2010.
4. Colone, F., K. Woodbridge, H. Guo, D. Mason, and C. J. Baker, "Ambiguity function analysis of wireless LAN transmissions for passive radar," *IEEE Transactions on Aerospace and Electronic Systems*, Vol. 47, No. 1, 240–264, 2011.
5. Colone, F., D. Langellotti, and P. Lombardo, "DVB-T signal ambiguity function control for passive radars," *IEEE Transactions on Aerospace and Electronic Systems*, Vol. 50, No. 1, 329–347, 2014.
6. Malanowski, M., K. Kulpa, J. Kulpa, P. Samczynski, and J. Misiurewicz, "Analysis of detection range of FM-based passive radar," *IET Radar, Sonar & Navigation*, Vol. 8, No. 2, 153–159, 2014.
7. Colone, F., R. Cardinali, and P. Lombardo, "Cancellation of clutter and multipath in passive radar using a sequential approach," *IEEE Conference on Radar*, 393–399, 2006.
8. Colone, F., R. Cardinali, P. Lombardo, and C. Ferretti, "Comparison of clutter and multipath cancellation techniques for passive radar," *IEEE Conference on Radar*, 469–474, 2007.
9. Zaimbashi, A., M. Derakhtian, and A. Sheikhi, "GLRT-based CFAR detection in passive bistatic radar," *IEEE Transactions on Aerospace and Electronic Systems*, Vol. 49, No. 1, 134–159, 2013.
10. Zaimbashi, A., M. Derakhtian, and A. Sheikhi, "Invariant target detection in multiband FM-based passive bistatic radar," *IEEE Transactions on Aerospace and Electronic Systems*, Vol. 50, No. 1, 720–736, 2014.
11. Bolvardi, H., M. Derakhtian, and A. Sheikhi, "Reduced complexity generalized likelihood ratio detector for digital broadcasting terrestrial-based passive radar," *IET Radar, Sonar & Navigation*, Vol. 9, No. 8, 1021–1029, 2015.
12. Zaimbashi, A., A. Sheikhi, and M. Derakhtian, "Evaluation of detection performance of passive bistatic radar detectors based on commercial FM radio signals," *Journal of Radar*, Vol. 1, No. 2, 23–34, 2014.
13. Stein, S., "Algorithms for ambiguity function processing," *IEEE Transactions on Acoustics, Speech and Signal Processing* , Vol. 29, No. 3, 588–899, 1981.
14. Neyt, X., J. Raout, M. Kubica, V. Kubica, S. Roques, M. Acheroy, et al., "Feasibility of STAP for passive GSM-based radar," *IEEE Conference on Radar*, 546–551, 2006.
15. Raout, J., A. Santori, and E. Moreau, "Passive bistatic noise radar using DVB-T signals," *IET Radar, Sonar & Navigation*, Vol. 4, , No. 3, 403–411, 2010.
16. Raout, J., A. Santori, and E. Moreau, "Space-time clutter rejection and target passive detection using the APES method," *IET Signal Processing*, Vol. 4, No. 3, 298–304, 2010.
17. Colone, F., R. Cardinali, P. Lombardo, O. Crognale, A. Cosmi, A. Lauri, et al., "Space-time constant modulus algorithm for multipath removal on the reference signal exploited by passive bistatic radar," *IET Radar, Sonar & Navigation*, Vol. 3, No. 3, 253–264, 2009.
18. Kay, S. M., *Fundamentals of Statistical Signal Processing*, Vol. 1, Prentice Hall, 1993.